Distinct magma evolution processes control the formation of porphyry Cu–Au deposits in thin and thick arcs

Chiaradia, Massimo

How to cite

CHIARADIA, Massimo. Distinct magma evolution processes control the formation of porphyry Cu–Au deposits in thin and thick arcs. In: Earth and planetary science letters, 2022, vol. 599, p. 117864. doi: 10.1016/j.epsl.2022.117864

This publication URL: https://archive-ouverte.unige.ch/unige:164514
Publication DOI: 10.1016/j.epsl.2022.117864

Earth and Planetary Science Letters 599 (2022) 117864

Contents lists available at ScienceDirect

Earth and Planetary Science Letters

www.elsevier.com/locate/epsl

Distinct magma evolution processes control the formation of porphyry Cu–Au deposits in thin and thick arcs

Massimo Chiaradia

Department of Earth Sciences, University of Geneva, Rue des Maraîchers 13, 1205-Geneva, Switzerland

ARTICLE INFO

Article history:
Received 14 March 2022
Received in revised form 29 September 2022
Accepted 5 October 2022
Available online xxxx
Editor: R. Hickey-Vargas

Keywords:
copper
gold
thin arc
thick arc
arc magma
modeling

ABSTRACT

Porphyry Cu–Au deposits are the major global source of copper, an essential metal for the green transition, and a significant source of gold. They occur both in thick continental and thin oceanic arcs at depths between ~1 and ~6 km above parental magma chambers situated at ~5–15 km depth. Although it is believed that the metal precipitation processes for these deposits are the same in thin and thick arcs, it is not clear why porphyry deposits in these two environments display different Cu and Au endowments and different Au/Cu ratios. Using mass balance petrological modeling, I argue that porphyry Cu–Au deposits in thick and thin arcs form by two distinct magmatic evolution precursors. In thick arcs porphyry Cu–Au deposits are tied to the deep crust build-up of large volumes of magmas, volatiles and metals. These large volumes of magmas are H_2O-undersaturated and need to rise to shallow level to exsolve fluids and metals. In contrast, porphyry Cu–Au deposits in thin arcs form by little differentiated mantle-derived magmas that rise directly to shallow crustal levels where they exsolve fluids and metals. These two distinct magmatic pathways of porphyry Cu–Au generation are ultimately controlled by the different arc thicknesses in the two environments, even though the processes of metal precipitation in the actual deposits of the shallow crust are similar. The model discussed here may stimulate the development of new tools for the exploration of porphyry deposits in the distinct environments of thick and thin arcs.

1. Introduction

Most porphyry Cu–Au deposits form in a syn-subduction arc emplaced upon thick (~30–60 km) continental crust and are associated with low- to medium-K calc-alkaline magmas (Sillitoe, 2010). However, in recent years, it has been recognized that world-class porphyry Cu–Au deposits also form in thin-intermediate (<~20–25 km thick) island arcs, particularly in post-subduction settings (Fig. 1), in association with both calc-alkaline magmas and variably alkaline magmas. Examples of these porphyry Cu–Au deposits are those formed recently in the SW-Pacific (e.g., Batu Hijau, Onto, and Elang, Indonesia; Tampakan, Philippines; Grasberg and OK Tedi, Papua New Guinea), and elsewhere in Mesozoic and Paleozoic times (e.g., Oyu Tolgoi, Mongolia; Cadia, Australia; Atlas, Philippines). Deposits in thin-intermediate arcs are characterized by a gold enrichment over copper (Au tons/Cu Mt ~80: *Au-rich porphyry Cu–Au type*) when compared to the syn-subduction (Andean) type formed on thick continental crust (Au tons/Cu Mt ~4: *Cu-rich porphyry Cu–Au type*) (Chiaradia, 2020, 2021a; Park et al., 2021). Additionally, deposits in thin-intermediate arcs also have the largest gold endowments of all porphyry Cu–Au deposits (from >500 to ~2600 tonnes Au: Batu Hijau, Onto, Cadia, Oyu Tolgoi, Grasberg), yet contain Cu endowments that allow their classification as giant (>3.16 Mt Cu) to supergiant (>10 Mt Cu) (Clark, 1993) porphyry-Cu deposits.

Whereas the processes that lead to metal precipitation in the shallow deposits (~1–6 km deep) of thin and thick arcs are considered to be similar (Richards, 2009), less attention has been given to possible differences in the precursor magmatic evolutions associated with porphyry Cu–Au deposits in these distinct geodynamic settings. This should be considered to improve exploration strategies of porphyry Cu–Au deposits adapting them to the different geodynamic environments of thin and thick arcs.

Here, I model petrological processes of magma evolution appropriate to thin versus thick arc environments using a Monte Carlo approach. Based on the model results, I discuss fundamental differences that could lead to the distinct Cu and Au endowments of porphyry Cu–Au deposits associated with thin and thick arcs and consequently to their distinct Au/Cu ratios, and compare model outputs with available data from various porphyry Cu–Au deposits around the world.

E-mail address: massimo.chiaradia@unige.ch.

https://doi.org/10.1016/j.epsl.2022.117864

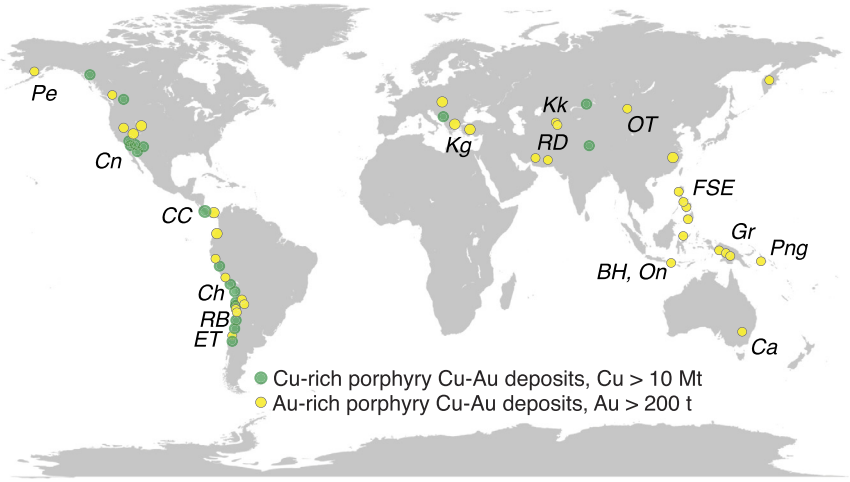

Fig. 1. Location of major Cu-rich (Au/Cu∼4) and Au-rich (Au/Cu∼80) porphyry Cu–Au deposits in syn- and post-subduction settings (modified after: Cooke et al., 2005; Richards, 2013). Abbreviations: BH = Batu Hijau; Ca = Cadia; CC = Cerro Colorado; Ch = Chuquicamata; Cn = Cananea; ET = El Teniente; FSE = Far South East-Lepanto; Gr = Grasberg; Kg = Kisladag; Kk = Kalmakyr; On = Onto; OT = Oyu Tolgoi; Pe = Pebble; RB = Rio Blanco; RD = Reko Diq. (For interpretation of the colors in the figure(s), the reader is referred to the web version of this article.)

2. Methods

Modeling has been carried out to estimate masses of magmas and of associated fluids and metals for two scenarios: (1) production of hybrid melts at different crustal levels following the equations developed by Chiaradia and Caricchi (2017) and Chiaradia (2020), and inspired by the hot-zone model of Annen et al. (2006), and (2) fractional crystallization of a mantle-derived basalt at different crustal levels. All simulations were carried out for depths ranging between ∼3.3 km (0.1 GPa) and ∼33.3 km (1.0 GPa) (Table S1).

According to the hot-zone model (Annen et al., 2006), hybrid magmas are produced in the crust from fractional crystallization, partial melting of the host crust and mixing with mantle-derived basalt. Hybrid magma productivity, i.e., the proportion of hybrid magma relative to the amount of injected basalt, increases with time at a fixed depth as the result of continuous thermal maturation. Additionally, magma productivity increases with depth in the crust, due to the increasing heat content of the crust with depth. Increasing magma productivity is accompanied by a progressive change of magma composition from felsic, at the beginning of the process, to increasingly intermediate with time (Annen et al., 2006).

The hot-zone model also shows that the incubation time, i.e., the time elapsed since the first basalt injection until a residual (felsic) melt from the fractionated basalt no longer solidifies, decreases with increasing depth because of the increasing heat content of the crust with depth.

Production of hybrid magmas in the crust was modeled for an average magma injection rate of 5 mm/y (Annen et al., 2006). Injection rate was translated into magma mass using the flux through a circular area of 8 km radius, a typical size of a magmatic reservoir accumulated in the crust (Annen, 2009; Schöpa and Annen, 2013), at any modeled depth (i.e., ∼3.3–33.3 km).

Fractional crystallization of basalt was carried out for fractionation from 100% to 15% residual melt. Mass of injected basalt was obtained using the same parameters as those used for the generation of hybrid melts (i.e., an average magma injection rate of 5 mm/y and a flux through a circular area of 8 km radius at any modeled depth).

Cumulative masses of hybrid and fractionating magmas and of associated aqueous fluids and metals were obtained considering timescales of fluid release by the above processes (1) and (2) dictated by those known for ore-forming processes at porphyry Cu–Au deposits (see below). For simplicity, H_2O has been considered as the only exsolved fluid (see also: Chiaradia and Caricchi (2022) for the potential effect of CO_2) and H_2O solubility has been modeled for pressure and melt composition dependency using the model of Newman and Lowenstern (2002). I have used a range of H_2O contents in the parental basalt (both calc-alkaline and alkaline) of 2–6 wt.%, which is typical of subduction-related primitive melts (Plank et al., 2013).

Cumulative masses of fluids were translated into masses of associated metals through fluid-melt K_D values (Table S1). The magmatic Cu and Au contents used varied depending on magma composition and depth of accumulation or fractionation (as shown by various studies; Figs. S1–S4). Magmatic Cu content dependency on degree and depth of magma differentiation was obtained from the data of Chiaradia (2014). The median Cu trend of thick arcs of Chiaradia (2014) was assigned a pressure of 1.0 GPa whereas that in thin arcs was assigned a pressure of 0.1 GPa. A continuous interpolation between these two extremes was obtained to assign specific Cu concentrations to magmas differentiating at intermediate depths (pressures) (Fig. S1). The same Cu content model was used for calc-alkaline and alkaline magma evolution.

Gold evolution in calc-alkaline magmas of thick arcs was obtained from Li et al. (2021) using fractional crystallization of 80% monosulfide-solid-solution (MSS) and 20% sulfide liquid (Fig. S2). Gold evolution in calc-alkaline magmas from thin arcs was modeled using the magmatic sulfur solubility model of Fortin et al. (2015) and assuming parental basalt concentrations of 500 ppm S (Wallace, 2005), 7.5 ppb Au (Moss et al., 2001), and an incompatible behavior of gold ($K_D = 0$) until the onset of magmatic sulfide saturation. After the onset of sulfide saturation (at MgO ∼4.5 wt.%) Au decrease is modeled using the Au curve of Li et al. (2021) for thin arcs (<20 km thickness) (Fig. S3).

For alkaline magmas a range of Au values between 10 and 32 ppb (Rock and Groves, 1988; Chiaradia, 2020) was allowed for any magma with MgO > 4.5 wt.%. For magmas with MgO < 4.5 wt.% the Au curve of Li et al. (2021) for thin arcs (<20 km thickness) was used (Fig. S4).

All raw metal endowments obtained by the simulations were reduced by precipitation efficiency values of 40–60% for Cu (Cloos, 2001) and 10–20% for Au (Chiaradia, 2020).

Modeling was carried out using a Monte Carlo approach because several parameters used in the equations are characterized

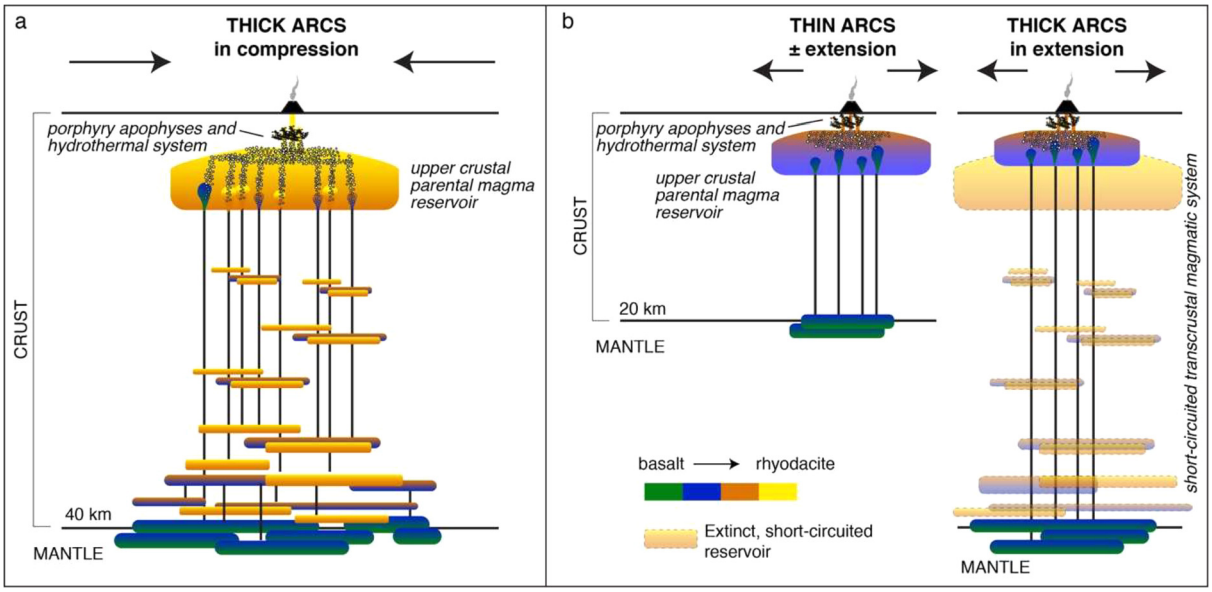

Fig. 2. (a) Transcrustal magmatic system in a thick arc under a dominant compressional tectonic regime. (b) Transcrustal magmatic systems in thin arcs and in thick arcs under an extensional tectonic regime. It is speculated that in thick arcs short periods of extension may lead to the short-circuiting of the transcrustal magmatic system formed during the long-lived compressional regime allowing the ascent of mantle-derived magmas from depth and their shallow-level differentiation. This regime could lead to the formation of Au-rich porphyry Cu–Au deposits in thick arcs by a similar process as those formed in thin-intermediate arcs (see text for further discussion).

by geologically possible ranges of values (see above and Table S1). Between 300000 and 500000 simulations were carried out using three scripts (Tables S2–S4) written with RStudio on the R environment (R Core Team, 2013).

3. Theory and calculation

3.1. Transcrustal magmatic systems in thick and thin arcs

Porphyry Cu–Au deposits are formed under volcanic edifices at convergent margin settings (Sillitoe, 1973). They are spatially and temporally associated with the construction of variably large upper crustal parental magma reservoirs emplaced between 5–15 km depth (Sillitoe, 2010) (Fig. 2). Finger-like porphyry apophyses propagate upwards from the parental magma reservoir and convey heat, aqueous fluids and metals (Fig. 2), resulting in mineralization at depths of ~1–6 km (Sillitoe, 2010).

The upper crustal magma reservoir is the forge of porphyry mineralization, but is only the uppermost expression of a much larger and deeper transcrustal magmatic system (Fig. 2) (Hildreth and Moorbath, 1988; Annen et al., 2006; Cashman et al., 2017), which, at convergent margins, results from prolonged flux of hot mantle-derived basalt into the overlying crust. Two end-member configurations of transcrustal magmatic systems characterize thick and thin arcs (Fig. 2). I choose a pressure limit of magma accumulation and differentiation of 0.6 GPa (corresponding to a depth of ~20 km) to differentiate between thin and thick arcs, appreciating that thick arc magmatism may extend to deeper levels (i.e., down to ~60 km), thin arc magmatism occurs at shallower levels, and intermediate situations occur in intermediate-thickness crust.

In thick arcs (corresponding to magma emplacement and evolution at depths >20 km), a mid- to lower crustal hybrid magma accumulation zone develops and grows through continuous long-lived basalt injection due to the increasingly high heat content of the crust at depths >20 km (Annen et al., 2006) (Fig. 2a). Long-lived compression in the overriding plate typically occurs during subduction (Richards, 2021) and slows down the ascent of mantle-derived melts, favoring their evolution at deep crustal levels. In agreement with this, geochemical indices of bulk rocks (e.g., increasing Sr/Y, La/Yb) indicate that magmas undergo an average deeper fractional crystallization as the arc crust thickness increases (Mantle and Collins, 2008; Profeta et al., 2015; Chiaradia, 2015, 2021b). This process results in the build-up of large volumes of hybrid magmas in thick arcs (Annen et al., 2006; Chiaradia and Caricchi, 2017) with a felsic-intermediate calc-alkaline composition (Fig. S5).

In thin arcs (corresponding to magma emplacement and evolution at depths <20 km), hybrid magmas will start to accumulate only after ~0.5 Myr of continuous basalt influx, due to the rapid cooling that mantle-derived basalt initially undergoes at shallow crustal levels (Annen et al., 2006). Additionally, porphyry Cu–Au deposits in thin-intermediate arcs are commonly associated with extension/trans-tension during late- to post-subduction (Hall, 2002; Redmond and Einaudi, 2010; Leys et al., 2012; Loucks, 2012). This further promotes the ascent of relatively undifferentiated mantle-derived magmas to shallow levels of an already thin crust (Tapster et al., 2016; Parra-Avila et al., 2022) (Fig. 2b), resulting in the volumetric predominance of mafic magmas compared to thick arcs (Fig. S5). In thin arcs, porphyry Cu–Au deposits are associated with both low-K and high-K calc-alkaline magmas as well as with alkaline magmas (Chiaradia, 2020).

3.2. Magmatic processes leading to fluid and metal exsolution in thin and thick arcs

The aqueous fluid and metal flux that can be supplied by a transcrustal magmatic system to form a porphyry Cu–Au deposit derive from two main petrogenetic processes associated with the crustal evolution of hydrous mantle-derived basalts:

1. Continuous basalt injection generates hybrid intermediate-felsic magmas, with size increasing through time and with depth of magma injection in the crust (see above). Fluid exsolution associated with the build-up of hybrid magmas is of two types:
   i. At $P < 0.6$ GPa and for accumulation times up to 3 Myr all hybrid magmas are H_2O-saturated and continuously exsolve an aqueous fluid (Fig. 3). This is a 1-step process because fluid exsolution occurs in the same place where hy-

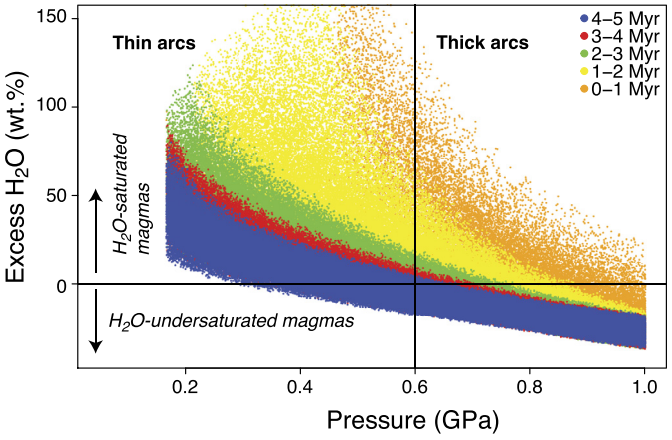

Fig. 3. Plot of excess H_2O (wt.%) versus pressure of hybrid magma accumulation. The plot shows that at P < 0.6 GPa (thin arcs) the majority of simulations for hybrid magmas correspond to H_2O-saturated systems, whereas at P > 0.6 GPa most hybrid magmas are H_2O-undersaturated. Color codes correspond to different durations of basaltic magma injection.

brid magma is formed and accumulated (*one-step continuous fluid exsolution from hybrid intermediate-felsic magmas*).

ii. At P > 0.6 GPa and for accumulation periods >3 Myr nearly all hybrid magmas are H_2O-undersaturated (Fig. 3). These magmas are only potentially fertile and need to exsolve their volatile and metal contents to become so. This can happen if the magma rises to shallower levels (the ~5–15 km interval of the parental magma reservoir) where it becomes H_2O-saturated (Chiaradia and Caricchi, 2017; Chiaradia, 2021a). This is a two-stage process because fluid exsolution occurs in a shallower place than where the hydrous hybrid magma is formed and accumulated (*two-stage fluid accumulation and exsolution from hybrid intermediate-felsic magmas*).

2. Combined with their role played in hybrid magma formation, mantle-derived basalt emplaced and fractionating at any depth in the crust may also exsolve fluids and metals by pressure-dependent or fractional crystallization-dependent H_2O saturation. Fig. 4a shows that at P < 0.6 GPa the majority of simulations of this process results in H_2O-saturation of the parental basalt depending on pressure of emplacement and/or subsequent crystallization even for relatively low H_2O initial contents (2–3 wt.%) and fractionation degrees (20%) (Fig. 4b). In contrast, at P > 0.6 GPa the majority of simulations results in H_2O-undersaturated magmas even for up to 50% fractionation (Fig. 4b) of basalt with initial H_2O contents up to 4 wt.% (Fig. 4a). Fig. 4c shows the probability distribution of H_2O saturation for more extreme pressure differences, highlighting how this process is dominant at low P (<0.4 GPa), typical of thin arcs, whereas it is nearly impossible at high P (>0.8 GPa), typical of thick arcs. The aqueous fluid exsolution associated with low-pressure magma emplacement and subsequent fractional crystallization can be considered typical of thin-intermediate arcs, where basalts evolve at shallow crustal levels (<~20 km, i.e., <~0.6 GPa) as dictated by the crustal thickness of thin-intermediate arcs and the extensional environment where magmas and the related porphyry Cu–Au deposits form (Fig. 2). This is a one-step process in which fluid exsolution occurs in the same place where magma is emplaced and differentiates (*one-step continuous shallow level exsolution of aqueous fluid from fractionating mafic-intermediate magmas*).

The amounts of aqueous fluids and metals that can be liberated by the three situations above (1a, 1b, 2) depend on the total mass of magma associated with each process. The total mass of magma, in turn, depends on (i) the rate at which magma is injected into the crust and/or hybrid magma is produced, (ii) the crustal section through which magma is fluxed, and (iii) the overall duration of the magma injection and/or hybrid magma formation process.

The rate of magma injection and size of the crustal section have been kept the same for all processes and all geodynamic settings to avoid additional variables and are typical of the construction of crustal magmatic reservoirs (see above). In contrast, available data indicate different timescales of the above-described processes. Overall durations of ore-forming processes in porphyry Cu–Au deposits range from tens to hundreds of thousands of years (Arribas et al., 1995; Marsh et al., 1997; Ballard et al., 2001; Cannell et al., 2005; Braxton et al., 2012; Deckart et al., 2013; Chelle-Michou et al., 2015; Buret et al., 2016; Large et al., 2018; Pollard et al., 2021). The longest durations (>1 Myr and nearly as long as 2 Myr) are recorded in the largest Cu-rich porphyry Cu–Au deposits (Ballard et al., 2001; Cannell et al., 2005; Deckart et al., 2013). Various studies (Ballard et al., 2001; Mercer et al., 2015; Chelle-Michou et al., 2017; Chiaradia and Caricchi, 2017; Chiaradia, 2020) have suggested that the overall duration of the ore-forming process determines the total endowment of the deposit, through the incremental, stepwise addition of magmas, fluids and metals to and their release from the shallow (5–15 km deep) parental magma reservoir (Fig. 2). Whereas the longest ore-forming durations (1–2 Myr) belong to the largest Cu-rich porphyry Cu–Au deposits in thick continental arcs, the maximum durations of ore-forming processes in the largest Au-rich porphyry Cu–Au deposits of thin arcs seem to be shorter (up to ~0.5 Myr) (Chiaradia, 2020). These different timescales are used for the quantification of the amounts of fluids and metals released by the three processes described above (1a, 1b, 2).

Processes 1a (*one-step continuous aqueous fluid exsolution from hybrid intermediate-felsic magmas*) and 2 (*one-step continuous shallow level aqueous fluid exsolution from fractionating mafic-intermediate magmas*) lead to a continuous release of fluids and metals from magmas upon emplacement and subsequent differentiation. This implies that the amount of fluids and metals associated with the volume of magma involved in such processes is limited by the maximum duration of ore formation. A conservative upper temporal limit of 0.5 Myr (0.4–0.6 Myr in the simulations) has been used for process 2, because this process is viable for thin-intermediate arcs where Au-rich porphyry Cu–Au deposits have maximum ore formation durations of ~0.5 Myr (Chiaradia, 2020).

Process 1a (*one-step continuous aqueous fluid exsolution from hybrid intermediate-felsic magmas*) may occur both in thin-intermediate arcs and thick arcs, on the different timescales of porphyry mineralizing processes discussed above (respectively <0.5 Myr and <2 Myr). Therefore, these temporal limits have been used for simulations of fluid and metal exsolution through process 1a.

In contrast, different timescales must be considered for the *two-stage fluid accumulation and exsolution from hybrid intermediate-felsic magmas* (1b), which consists of an initial deep-level magma and fluid accumulation stage, followed by a shallow-level fluid exsolution stage, with independent timescales. As discussed above, process 1b cannot occur in thin-intermediate arcs, because deep fluid accumulation becomes significant only for P > 0.6 GPa (Fig. 3). Whereas maximum duration of ore deposition in thick arcs for Cu-rich porphyry Cu–Au deposits is <2 Myr (see above), accumulation of the hybrid magma (and its fluid and metal content) in the deep crust can be much longer. Geochronological evidence exists for several Myr (4–6 Myr) accumulations of magmas associated with the formation of Cu-rich porphyry Cu–Au deposits in thick arcs (Reich et al., 2003; Chiaradia et al., 2009; Stern et al., 2011; Chelle-Michou et al., 2014; Rabbia et al., 2017). A limit of 5 Myr has been used in the simulations for the accumulation of magmas in the deep crust.

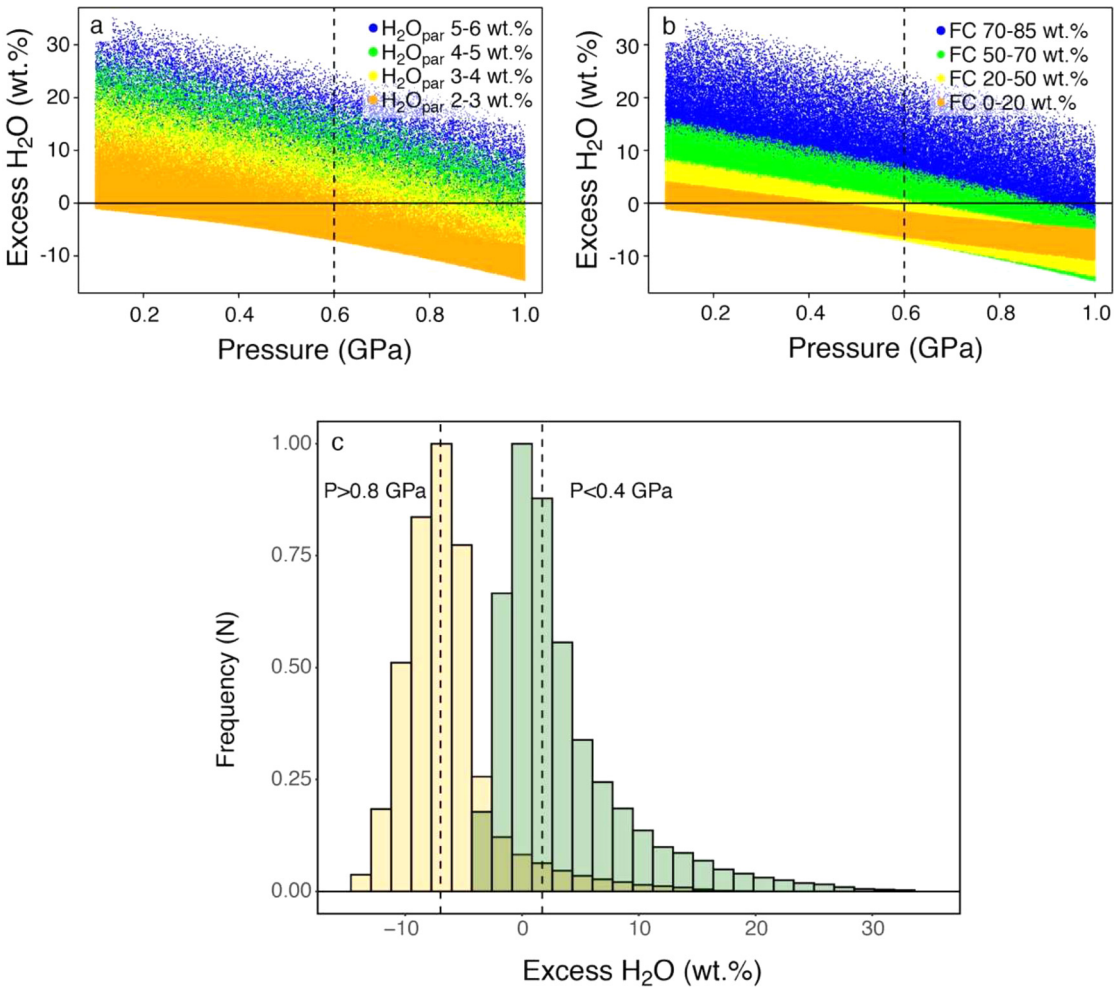

Fig. 4. (a–b) Plot of excess H_2O (wt.%) versus pressure for basaltic magma fractionating (from 100 to 15% residual melt fraction) at different pressures. Color codes correspond to different H_2O contents in the parental basalt (a) and different degrees of fractional crystallization (b). (c) Histogram of the relative frequency distribution of excess H_2O in basalts emplaced and fractionating at P > 0.8 GPa (thick arcs) and <0.4 GPa (thin arcs). Negative values of excess H_2O indicate H_2O-undersaturated conditions whereas positive values indicate H_2O-saturated conditions.

4. Results

4.1. Cu and Au endowments in thin and thick arcs modeled with process 1a

The plots of Fig. 5 show the Cu and Au endowments associated with exsolution of the excess fluid component of fluid-saturated hybrid calc-alkaline magmatic systems accumulating at different pressures during up to 5 Myr (process 1a: *one-step continuous aqueous fluid exsolution from hybrid intermediate-felsic magmas*).

The largest Cu (up to 80 Mt) and Au (up to 35 tons) endowments occur after 4–5 Myr of continuous aqueous fluid exsolution from these magmas, and could explain the Cu endowments of several large Cu-rich porphyry Cu–Au deposits (Fig. 5). However, the ore-forming durations of these deposits are ≤~1.5 Myr (Stein et al., 2002; Dilles et al., 2004; Zimmerman et al., 2014), which corresponds to maximum simulated Cu and Au endowments of <10 Mt Cu and <5 tons Au at any pressure higher than ~0.4 GPa. Therefore, such a process could at best explain maximum Cu endowments of ~10 Mt Cu and insignificant Au endowments. Additionally, the maximum potential endowments occur for systems that are continuously exsolving fluids at high pressures (>~0.6 GPa) for durations of ~1.5 Myr (Fig. 5); it is unlikely that fluids exsolving so deep can be focused into the same upper crustal volume during 100 s of kyr and up to ~1.5 Myr to form an economic deposit (Richards, 2021). Therefore, process 1a is overall unlikely to form porphyry Cu–Au deposits of any size. Fig. 5 shows that process 1a cannot contribute any Cu and Au endowment in thin-intermediate arcs (<0.6 GPa) since they are formed in even shorter timescales (<~0.5 Myr) for which Cu and Au endowments associated with this process are insignificant, because no hybrid magmas can be formed in such short timescales at these low pressures.

4.2. Cu and Au endowments in thin and thick arcs modeled with process 1b

Fig. 6 shows that the amounts of copper and gold that can potentially be released (i.e., exsolvable) by H_2O-undersaturated calc-alkaline hybrid magmas (process 1b: *two-stage fluid accumulation and exsolution from hybrid intermediate-felsic magmas*) steadily increase with pressure of hybrid magma formation and accumulation. This is the combined effect of the increase with depth of H_2O solubility (Newman and Lowenstern, 2002) and of the mass of accumulated magma (Annen et al., 2006; Chiaradia and Caricchi, 2017). Accordingly, the plots show that copper and gold endowments associated with such a process become significant only for P > ~0.4 GPa, because at lower pressures most of the fluids and metals are lost by hybrid magmas through continuous fluid exsolution (process 1a above; Fig. 3). Such a process, therefore, applies to thick arcs.

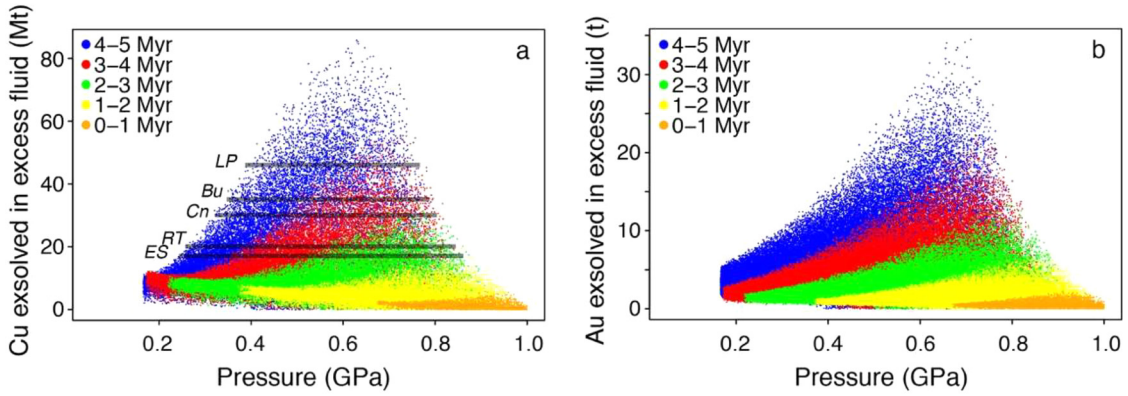

Fig. 5. Plots of potential Cu (40–60% precipitation efficiency) (a) and Au (precipitation efficiency 10–20%) (b) endowments associated with continuous exsolution of excess H_2O (wt.%) from hybrid magmas at different pressures. Color codes indicate duration intervals of the exsolution process. The simulations show a peak in the potential Cu and Au endowments associated with this process at around 0.6 GPa, in correspondence with the longest injection time interval (4–5 Myr). This is due to the antithetic behaviors of the total amounts of Cu and Au in the hybrid magma and the excess H_2O in the hybrid magmatic systems at different depths (Fig. S6). Total copper and gold in the hybrid magmas decrease with decreasing P because they correspond to hybrid magmatic systems progressively more differentiated (Figs. S1–S4) and of smaller size (Annen et al., 2006; Chiaradia and Caricchi, 2017). Additionally, Cu and especially Au contents are very low in more differentiated (Chiaradia, 2014; Li et al., 2021), shallower and smaller hybrid magmatic systems (Figs. S1–S4). In contrast, the amount of excess H_2O steadily increases with decreasing pressure (Fig. S6). For comparison also shown in Fig. 5a are the Cu endowments of several deposits from Chiaradia (2020) and references therein. No Au endowments of economic deposits are shown in Fig. 5b because they fall at significantly higher values than those of the simulations. Abbreviations: Bu = Butte; Cn = Cananea; ES = El Salvador; LP = Los Pelambres; RT = Radomiro Tomic.

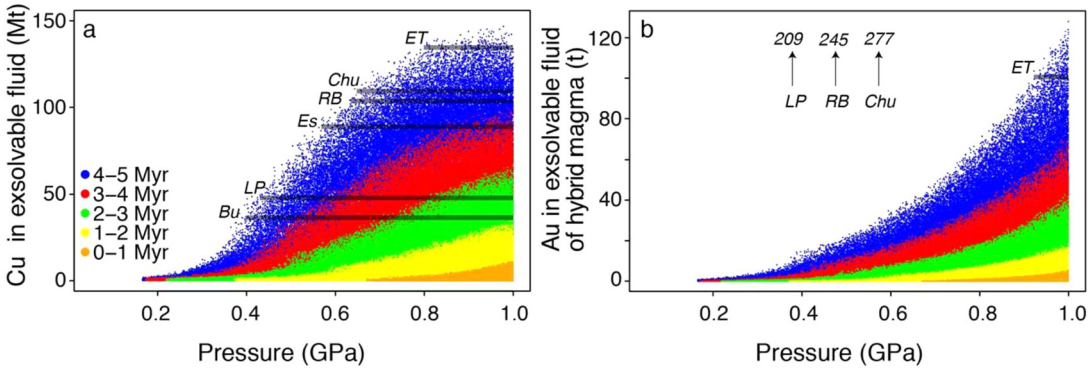

Fig. 6. Plots of potential Cu (40–60% precipitation efficiency) (a) and Au (precipitation efficiency 10–20%) (b) endowments associated with accumulation of H_2O-undersaturated hybrid magmas at different pressures. Color codes indicate duration intervals of the accumulation process. The Cu and Au endowments of the deposits are from Chiaradia (2020) and references therein. Abbreviations: Bu = Butte; Chu = Chuquicamata; Es = Escondida; ET = El Teniente; LP = Los Pelambres; RB = Rio Blanco-Los Bronces.

The plots of Fig. 6 also show the strong control of the duration of magma injection on the amount of exsolvable metals (Chiaradia and Caricchi, 2017). The largest potential endowments (>50 and up to ~150 Mt Cu), that could explain the observed Cu endowments of the largest Cu-rich porphyry Cu–Au deposits (e.g., those of Chile), are associated with long-lived (>3 Myr) and deep (>0.6 GPa) hybrid calc-alkaline magma systems (Fig. 6a). As discussed above, such large amounts of Cu can be released only when deep crustal hybrid magmas rise to the shallow parental magma reservoir where they can deliver their fluid and metal content within the timeframe of porphyry mineralization (i.e., <2 Myr, and mostly <~1 Myr).

Gold potentially exsolvable from these undersaturated hybrid magmas reaches a maximum of ~120 tons in the simulations (Fig. 6b). This is on the same order of magnitude as (albeit a factor of two lower than) the maximum Au endowments (up to ~270 tons Au) of Cu-rich porphyry Cu–Au deposits of thick arcs (Fig. 6b). The resulting [Au t/Cu Mt] ratios range from near 0 to ~10 (Fig. S7), i.e., they are similar to those (~4) of Cu-rich porphyry Cu–Au deposits of Chiaradia (2020). This process cannot explain the Au endowments (~500->1000 tons Au) of several Au-rich calc-alkaline porphyry Cu–Au systems of thin-intermediate island arcs (FSE, Philippines; Batu Hijau and Onto, Indonesia) and of thick arc settings (Cerro Casale, Chile; Cascabel, Ecuador; Minas Conga, Peru; Reko Diq, Pakistan), nor their high Au/Cu ratios around 100 (see below).

4.3. Cu and Au endowments in thin and thick arcs modeled with process 2: calc-alkaline magmas

Potential Cu and Au endowments associated with excess fluid exsolution from a fractionating calc-alkaline mafic-intermediate magma (process 2: *one-step continuous shallow level aqueous fluid exsolution from fractionating mafic-intermediate magmas*) become significant only at P < ~0.6 GPa and reach maximum values (~70 Mt Cu, ~1500 tonnes Au) at P ~ 0.1–0.3 GPa (Fig. 7). This process, therefore, applies to magma evolutionary processes in thin-intermediate arcs (Fig. 2). For this reason, a maximum injection period interval of 0.4–0.6 Myr (simulating the longest ore-forming timescales of ~0.5 Myr in thin arcs: see above) has been used in the simulations related to this process in thin-intermediate arcs.

The simulations associated with this fluid exsolution process largely explain the Cu (5–15 Mt) and Au (up to ~1000 tonnes Au) endowments of the largest calc-alkaline Au-rich porphyry Cu–Au deposits in thin-intermediate arcs (Figs. 7a–d).

Simulations also show (Figs. 7a, 7c) that, whereas the highest Cu endowments of Au-rich porphyry Cu–Au deposits in thin-intermediate arcs can be explained by any H_2O contents in the parental magma (i.e., 2–6 wt.%), the highest Au endowments in the

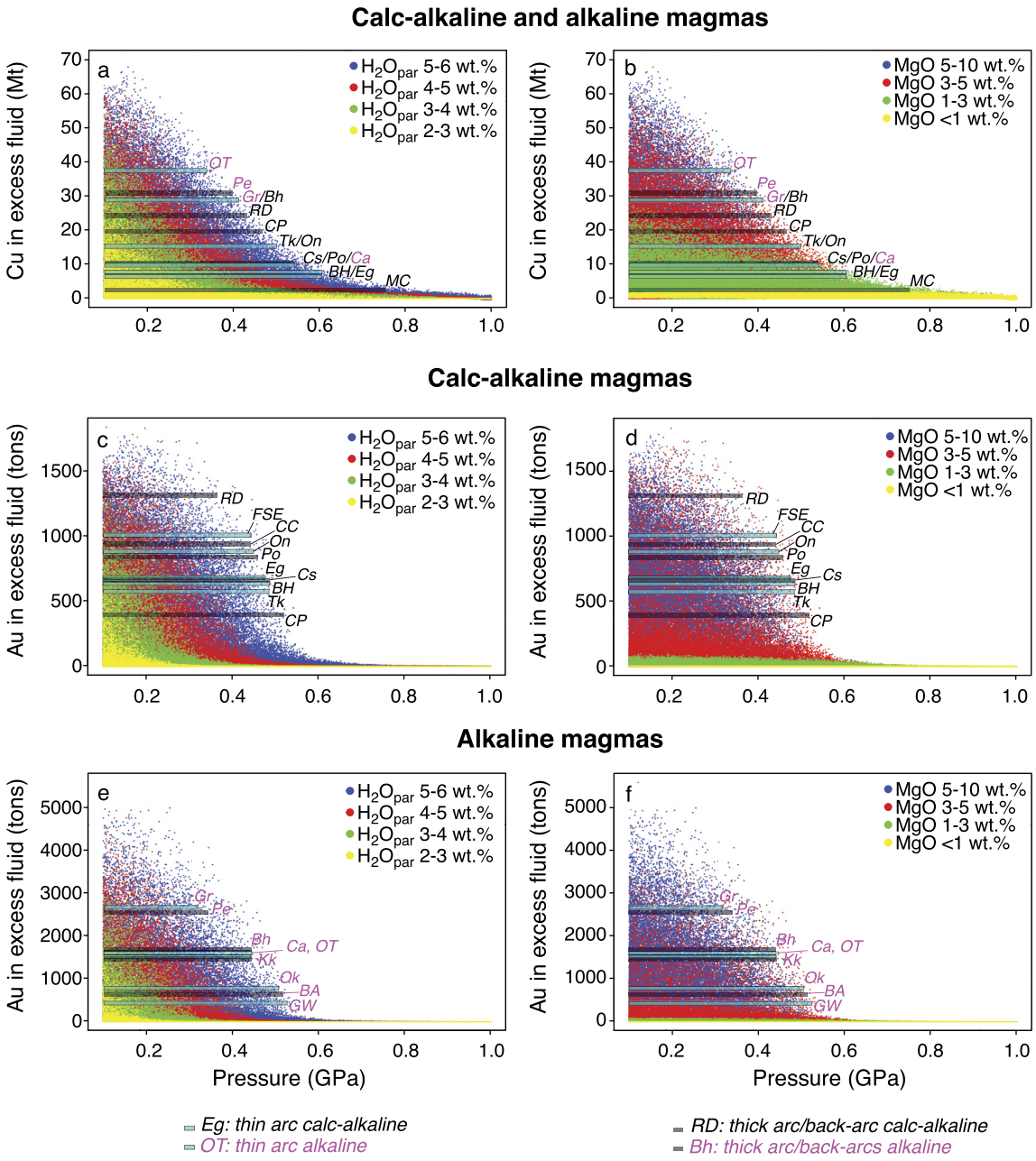

Fig. 7. (a–b) Plots of potential Cu (40–60% precipitation efficiency) endowments associated with continuous fluid exsolution from fractionating calc-alkaline and alkaline basalt at different pressures. (c–d) Plots of potential Au (10–20% precipitation efficiency) endowments associated with continuous fluid exsolution from fractionating calc-alkaline basalt at different pressures. (e–f) Plots of potential Au (10–20% precipitation efficiency) endowments associated with continuous fluid exsolution from fractionating alkaline basalt at different pressures. Endowments are cumulate values resulting from injection of basalt at an average rate of 5 mm/y during 0.4–0.6 Myr. Simulations are color-coded for initial H_2O contents of the parental basalt (a, c, e) and its degree of fractionation, i.e., MgO contents of the residual melt (b, d, f). The Cu and Au endowments of the Au-rich porphyry Cu–Au deposits are from (Chiaradia, 2020) and references therein except Cascabel (Cs) which is from (Vaca et al., 2019). Abbreviations: BA = Bajo de la Alumbrera; Bh = Bingham; BH = Batu Hijau; Ca = Cadia; CC = Cerro Casale; CP = Cobre Panama; Cs = Cascabel; Eg = Elang; FSE = Far South East-Lepanto; Gr = Grasberg; GW = Golpu-Wafi; Kk = Kalmakyr; MC = Minas Conga; Ok = Ok Tedi; On = Onto; OT = Oyu Tolgoi; Pe =Pebble; Po = Potrerillos; RD = Reko Diq; Tk = Tampakan.

same deposits require higher H_2O contents in the parental magma (4–6 wt.%). This might suggest that the combined Au and Cu endowments of these deposits require H_2O contents on the highest side of the range of subduction-related basalts for this type of process. Speculating, such enrichment could be related to the peculiar late- to post-subduction geodynamic environment of formation of these deposits, and therefore of their parental basalts (Fiorentini and Garwin, 2010; Fiorentini et al., 2018).

Figs. 7b and d show that any magma with MgO $\geq$ 1 wt.% can potentially deliver the amounts of Cu observed in the largest Au-rich porphyry Cu–Au deposits of thin arcs. However, magmas with MgO > 3 wt.% and even >5 wt.% are required to explain the largest Au endowments in the same deposits. This is due to the strong depletion of Au in magmas below ~4.5 wt.% in thin arcs (Li et al., 2021), which makes fluids exsolving from them also strongly depleted in Au (Park et al., 2019, 2021).

The simulations of the one-step continuous shallow level aqueous fluid exsolution from fractionating mafic-intermediate calc-alkaline magmas are also able to explain the Au and Cu endowments of calc-alkaline Au-rich porphyry Cu–Au deposits formed in thick continental arcs, like Cerro Casale, Cascabel, and Reko Diq (Figs. 7a–d).

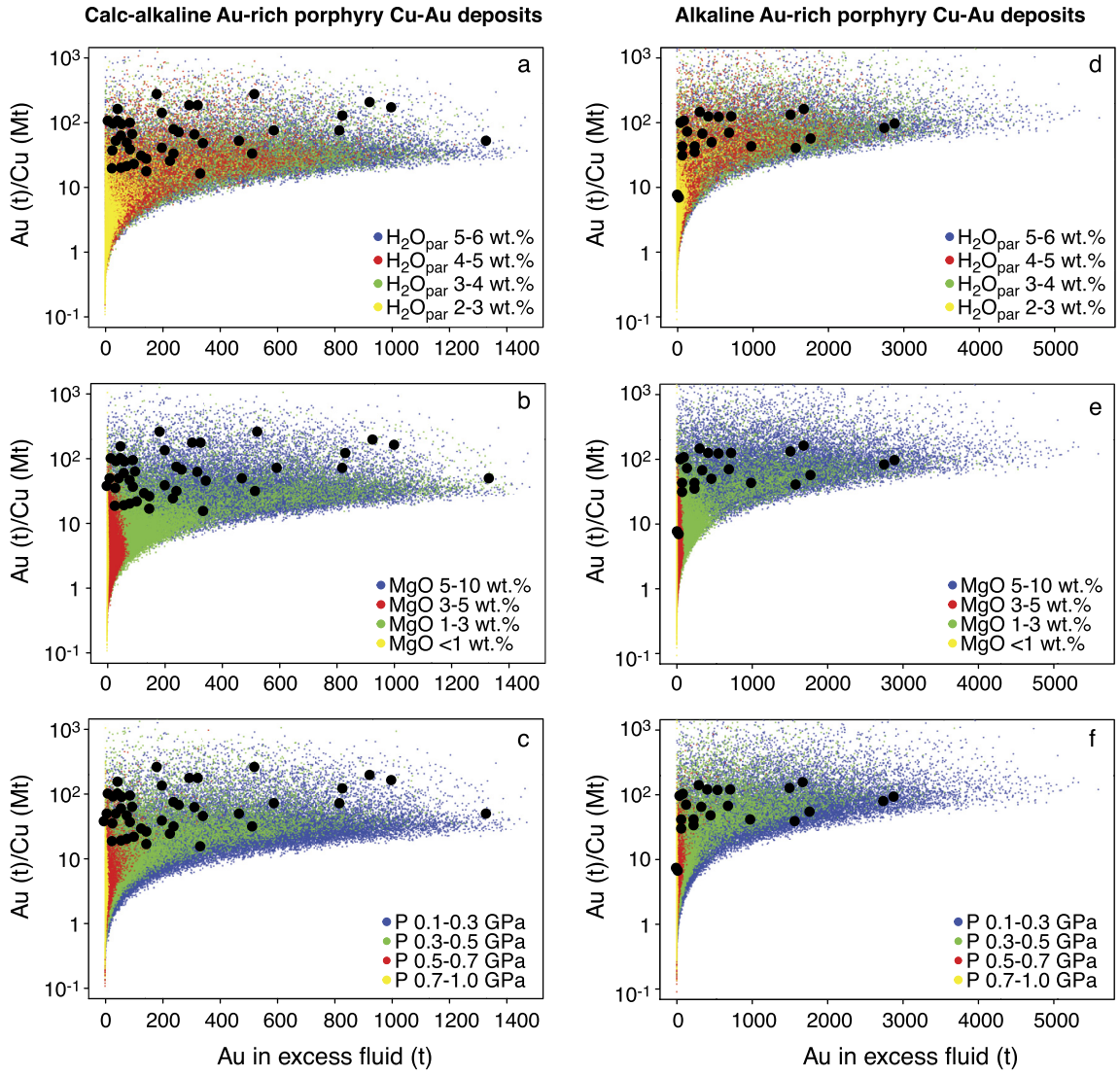

Fig. 8. Plots of the simulations of Au (t)/Cu (Mt) values versus Au endowments associated with excess fluids from fractionating calc-alkaline (a–c) and alkaline (d–f) basalt at different pressures. Endowments are cumulate values resulting from injection of basalt at an average rate of 5 mm/y during 0.4–0.6 Myr. Simulations are color-coded for initial H_2O contents of the parental basalt (a, d), its degree of fractionation, i.e., MgO contents of the residual melt (b, e), and pressure of basalt emplacement and differentiation (c, f). Black dots are Cu and Au endowments and their ratios of Au-rich porphyry Cu–Au deposits from (Chiaradia, 2020) and references therein.

Figs. 8a–c show that Au/Cu ratios of calc-alkaline Au-rich porphyry Cu–Au deposits fall in the range of the simulations, albeit plotting at slightly higher values than the bulk of the simulations. This could be the (subordinate?) effect of additional processes that were not considered in the modeling, like gold recycling from Au-rich sulfides in the lower crust (Shafiei et al., 2008; Richards, 2009; Holwell et al., 2022) or Au precipitation efficiencies higher than the range here simulated (Table S1). Figs. 8a-c show again that the largest Au-rich porphyry Cu–Au deposits are preferentially associated with parental basalts having H_2O values on the higher side of the range of subduction-related basalts (2–6 wt.%), displaying lower fractionation degrees (i.e., higher MgO), and differentiating at the shallowest depths (0.1–0.3 GPa).

4.4. Cu and Au endowments in thin and thick arcs modeled with process 2: alkaline magmas

Simulations carried out for calc-alkaline systems (Figs. 7a-d) fail to explain the exceptionally high Au endowments of alkaline systems (Figs. 7e–f). Instead, simulations carried out using the higher Au contents of mafic alkaline magmas (10–32 ppb) (Rock and Groves, 1988; Chiaradia, 2020) are able to explain the Au endowments of alkaline porphyry Cu–Au deposits in thin-intermediate arcs (Figs. 7e–f).

Also in this case, as for calc-alkaline systems, high parental H_2O contents (4–6 wt.%) as well as limited fractionation (MgO > 3–5 wt.%) at increasingly shallow levels are required by the simulations to reproduce the combined Cu and Au endowments of the largest alkaline-related Au-rich porphyry Cu–Au deposit (e.g., Grasberg, 2600 t Au: Figs. 7e–f, 8d–f). This is consistent with the genesis of alkaline magmas in a post-subduction, post-collisional setting by small degrees partial melting of a metasomatized lithospheric mantle resulting in high initial H_2O contents and alkaline composition of the parental basalts (Fiorentini et al., 2018). The simulations of alkaline systems that exsolve aqueous fluids at shallow levels are also able to explain the Au and Cu endowments of alkaline-related Au-rich porphyry systems in other extensional geodynamic settings, like Bingham Canyon, Kalmakyr, and Pebble (Figs. 7e–f).

The plots of Figs. 8d–f show that simulations for alkaline systems reproduce remarkably well the Au/Cu ratios of alkaline-related Au-rich porphyry Cu–Au deposits.

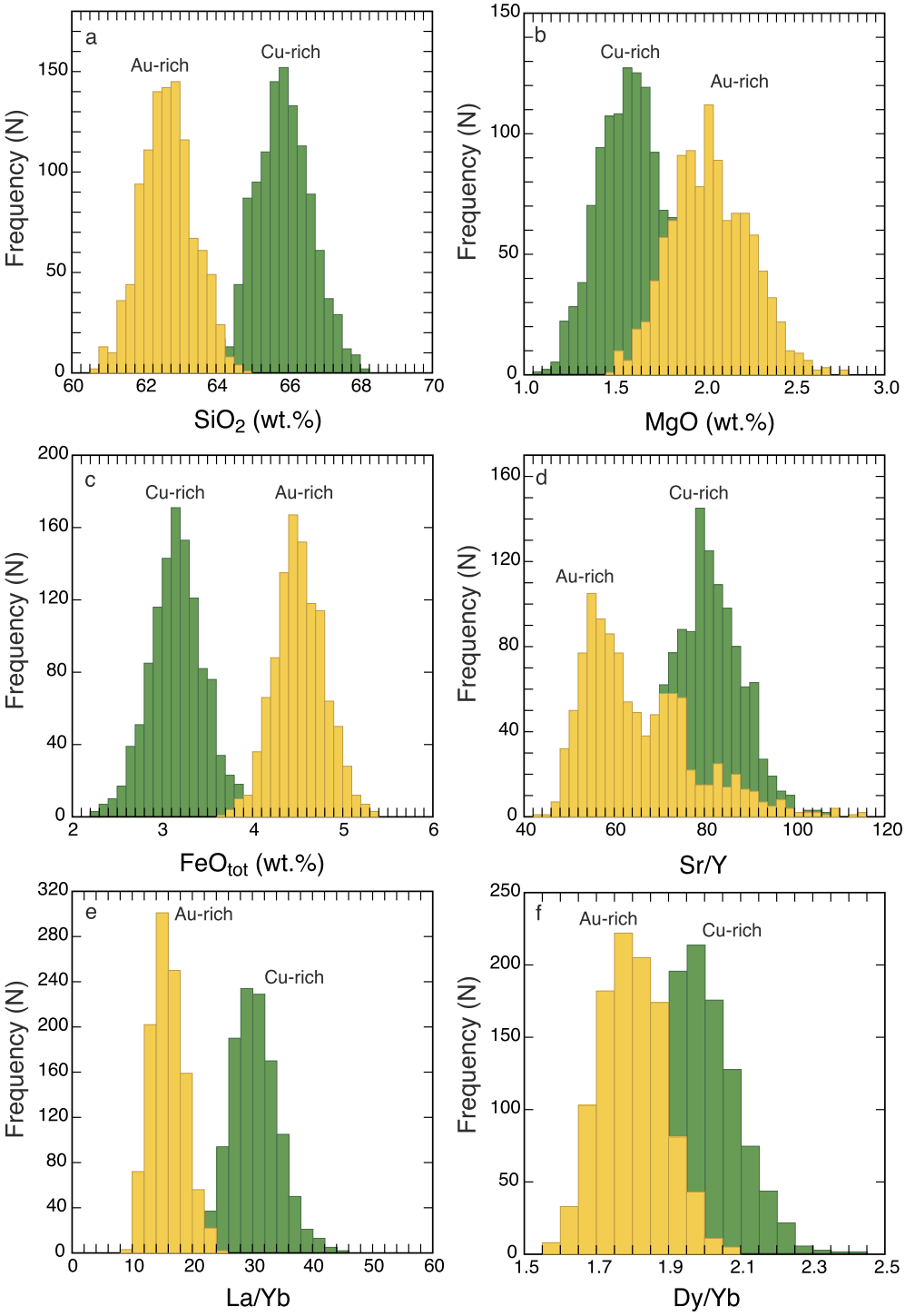

Fig. 9. Frequency histograms showing the compositional differences of magmatic rocks associated with Cu-rich and Au-rich porphyry Cu–Au deposits for SiO_2 (a), MgO (b), FeO_{tot} (c), Sr/Y (d), La/Yb (e), and Dy/Yb (f). The data used for the frequency histograms are from bootstrap resampling of the database of (Loucks, 2014). Bootstrap resampling was carried out to increase the statistical significance of the dataset (see Supplementary Material Dataset S1).

5. Discussion

5.1. Different geochemical compositions of magmas associated with porphyry Cu–Au deposits in thin and thick arcs

Fig. 9 shows that distinct geochemical features characterize magmatic rocks associated with either Au-rich or Cu-rich porphyry Cu–Au deposits. The data plotted in Fig. 9 are from bootstrap resampling of the data of Loucks (2014). Such a procedure has been adopted to increase the statistical significance of the two datasets (see Supplementary Material Dataset S1). Figs. 9a–b show that magmatic rocks associated with Au-rich porphyry Cu–Au deposits are more primitive (mode values of SiO_2 and MgO at ~63 and ~2 wt.%, respectively) than those associated with Cu-rich porphyry Cu–Au deposits (mode values of SiO_2 and MgO at ~66 and ~1.5 wt.%, respectively), as predicted by the model results presented above. Nonetheless the mode of the MgO values of magmatic rocks associated with Au-rich porphyry Cu–Au deposits (~2 wt.%) is somewhat lower than that expected from the

model above discussed (>3 wt.%). This could be due to the fact that the porphyry fingers that host the mineralization, and are usually sampled in porphyry Cu–Au deposits, are more differentiated than the underlying degassing magma reservoir. Additionally, in alkaline and high-K calc-alkaline magmatic systems, which form the largest Au-rich porphyry Cu–Au deposits, sulfide saturation occurs at a more advanced stage of differentiation than in calc-alkaline system (Li et al., 2019) allowing Au to be exsolved into the fluid phase from more evolved magmas than typical calc-alkaline magmas here used to model Au contents during differentiation (Li et al., 2021). Figs. 9c–e highlight two further significant features of magmas associated with Au-rich porphyry Cu–Au deposits: (i) they have significantly higher FeO_{tot} contents due to their less evolved composition but also to the retarded magnetite crystallization in thin arcs which results in a retarded sulfide saturation (Chiaradia, 2014); (ii) they are characterized by lower Sr/Y, La/Yb and Dy/Yb values suggesting an overall shallower magma evolution, which is consistent with the conceptual model discussed above. The above differences in geochemical compositions of magmas associated with either Au-rich or Cu-rich porphyry Cu–Au deposits are in agreement with recent data presented by Hao et al. (2022).

5.2. Distinct models for porphyry Cu–Au deposits in thick and thin arcs

Porphyry Cu–Au deposits are the complex result of geochemical, petrological, geodynamic, and tectonic processes and their timescales (Richards, 2003; Wilkinson, 2013). The modeling presented above provides a mass-balance framework within which discuss such processes and needs further testing by geochemical, petrological, geochronological, tectonic, and geodynamic studies on individual porphyry Cu–Au deposits. The above data indicate that the distinct endowments and Au/Cu ratios of Au-rich and Cu-rich porphyry Cu–Au deposits can be explained by two end-member magmatic evolution and fluid-metal exsolution processes. The geological value of the modeling is that the occurrence of either one of the two processes can be tied to the different crustal architectures and geodynamic settings in which Au-rich and Cu-rich porphyry Cu–Au deposits occur (Fig. 2).

Cu-rich porphyry Cu–Au deposits (up to >100 Mt Cu but less than 300 tons of Au) occur in thick arcs and have low (~4) Au/Cu ratios (Chiaradia, 2020). The simulations discussed above show that, among those considered here, the only end-member process able to reproduce these endowments and their relative ratios is the *two-stage fluid accumulation and exsolution from hybrid intermediate-felsic magmas* (process 1b).

This two-stage process is consistent with the unique crustal architecture, geodynamic, tectonic, geochronological, and geochemical features of the thick, syn-subduction continental arc magmatic systems associated with Cu-rich porphyry Cu–Au deposits. The thick crust of continental arcs and the long periods of compression on the overriding plate that are associated with syn-subduction geodynamic processes (Richards, 2021) offer the ideal framework for accumulation of magmas and fluids in the deep crust. Prolonged magma evolution at deep crustal levels results in the typical high Sr/Y (and other indices: La/Yb, V/Sc) values that are a hallmark for Cu-rich porphyry Cu–Au deposits (Richards, 2011; Chiaradia et al., 2012; Loucks, 2014; Chiaradia and Caricchi, 2017). The decoupling between Cu and Au in Cu-rich porphyry Cu–Au deposits is due to the early magmatic sulfide saturation occurring at deep crustal levels of a thick crust (Chiaradia, 2014; Matjuschkin et al., 2016; Hao et al., 2022). Because Au is much more chalcophile than Cu (Ripley et al., 2002; Li and Audétat, 2013), the loss of Au in the deep hybrid magma is nearly quantitative (Li et al., 2021). In contrast, Cu remains in the magma in concentrations sufficient to form even behemothian (>31.16 Mt Cu)(Clark, 1993) porphyry Cu deposits, because the Au loss is compensated by the large magma volumes accumulated at deep crustal levels. Further decoupling may also occur due to different precipitation efficiency at differently shallow crustal levels (Chiaradia, 2020). The occurrence of porphyry Cu–Au deposits at the end of long periods of compression and at the transition to near-neutral stress conditions in the thick crust (Richards, 2003; Bertrand et al., 2014) offers the ideal framework for the focused transfer of the large magma accumulations from the deep crust to shallower levels through transcrustal tectonic structures (Richards, 2021). Repeated focused and pulsed transfer of the large magma accumulations from the lower crust to the upper crust parental magma reservoir results in the incremental exsolution of fluids and accumulation of metals in timescales as long as 1–2 Myr.

Au-rich porphyry Cu–Au deposits contain up to ~30 Mt Cu and ~2600 tons Au and have high Au/Cu ratios (~80–120) (Fig. 8). Mass-balance simulations show that, among those here considered, the only magmatic process able to reproduce these endowments and Au/Cu ratios is continuous aqueous fluid exsolution from little differentiated mantle-derived magmas fractionating at shallow crustal levels (process 2).

Although no detailed geological and tectonic setting characterization exists for all Au-rich porphyry Cu–Au deposits, a feature common to all those for which information exists is the occurrence of trans-tensional to extensional tectonics during syn-mineral magmatism (Garwin, 2002; Hall, 2002; Redmond and Einaudi, 2010; Leys et al., 2012; Burrows et al., 2020). These tectonic regimes favor ascent of magma with little interaction with the crust and emplacement and evolution at shallow depths (Cembrano and Lara, 2009). Therefore, despite the variety of magma compositions (low-K calc-alkaline, high-K calc-alkaline, alkaline) and geodynamic settings (late- to post-subduction in thin to intermediate island arcs, back-arcs, thick arcs) associated with Au-rich porphyry Cu–Au deposits, a common point that stems out is an overall shallower magma emplacement and evolution (see also: Chiaradia, 2020; Hao et al., 2022).

Aqueous fluid exsolution from little differentiated mantle-derived magmas fractionating at shallow crustal levels (process 2) is congenital in thin-intermediate arcs, where the thin crust (<~20–25 km) makes impossible a high-pressure evolution of magmas, and syn-mineral magmatism during late-to post-subduction trans-tension/extension further favors the rapid ascent of little differentiated magmas and their evolution at shallow depth. One could speculate that the same process could also occur in thicker crust, both in extensional back-arc setting, e.g., Bingham (Redmond and Einaudi, 2010), or during short-lived periods of extension in thick arcs, e.g., Maricunga belt (Kay et al., 1994), leading to the formation of Au-rich porphyry Cu–Au deposits also in thick crust. Short periods of extension within the dominant long-lived compressional regime of thick arcs could favor the short-circuiting of the deep hot zone leading to a configuration similar to that of thin arcs (Fig. 2b). More information needs to be gathered on these deposits to test the applicability of this model to them.

The simulations also reproduce the higher gold endowments of alkaline-related Au-rich porphyry Cu–Au deposits as a consequence of higher initial Au contents in alkaline magmas (Figs. 7e–f). As pointed out by previous studies (Rock and Groves, 1988; Jensen and Barton, 2000; Sillitoe, 2000; Chiaradia, 2020) this suggests a petrogenetic control on the gold endowments of alkaline-related Au-rich porphyry Cu–Au deposits.

Continuous fluid exsolution from mantle-derived magmas fractionating at shallow depths optimally exploits two advantages of the thin-intermediate arc environment to form giant to supergiant porphyry Cu deposits (>5 and up to 30 Mt Cu) with the largest Au endowments (~500–2600 t Au) among all porphyry Cu–Au deposits known. The first advantage is the significantly higher Cu and Au contents of intermediate magmas in thin versus thick arcs

(Figs. S1–S4), due to delayed magmatic sulfide saturation in thin arcs (Chiaradia, 2014; Li et al., 2021). The second one is the exsolution of fluids at an earlier stage of magma differentiation than in thick arcs (Chiaradia, 2021a, 2021b; Park et al., 2021; Hao et al., 2022). This is due to the ascent of little differentiated hydrous magmas to shallow levels where H_2O solubility is lower (Newman and Lowenstern, 2002) and a large amount of fluid can be exsolved before Cu and especially Au are removed by sulfides in the differentiating magma (Park et al., 2019; Hao et al., 2022). Even if sulfide melt saturation might occur at the base of a 20–25 km thick crust (Holwell et al., 2022), early H_2O saturation of hydrous magmas in thin-intermediate arcs (Fig. 4) could favor the transport of Cu- and Au-rich melt droplets to shallow levels by flotation on vapor bubbles exsolved by the magma (Mungall et al., 2015). Such process is not possible in thick arcs, where H_2O saturation is not reached at lower crustal depths (Fig. 4).

Simulations show (Fig. 7) that the most fertile magmatic systems exsolving aqueous fluids at shallow levels are those with higher initial H_2O contents (>3–4 wt.%) and not too differentiated (MgO > 3 wt.%). These outcomes of the modeling are consistent with conclusions of previous studies (Fiorentini and Garwin, 2010; Loucks, 2014; Parra-Avila et al., 2022) and with the generally less evolved chemical composition of magmas of thin arcs in general (Fig. S5) and of magmas associated with Au-rich porphyry Cu–Au deposits in particular (Fig. 9), although MgO values returned by the model are somewhat higher than real data (Fig. 9b). Like for Cu-rich porphyry Cu–Au deposits (Chiaradia and Caricchi, 2017), geological and geochronological evidence suggests an incremental stepwise build-up of the Au-rich porphyry Cu–Au deposits over timescales of up to a few hundreds of kyr (Chiaradia, 2020).

Favorable magma chemical composition (high initial H_2O, high Cu and Au contents, eventually alkalinity), geodynamic features (thin crust, extension), and short periods of fertile magmatism seem to occur together in the late- to post-subduction and post-collision setting of thin-intermediate arcs. This might be due to the fact that in this setting temporally short windows of asthenospheric mantle upwelling cause transient periods of partial melting of asthenospheric mantle, lithospheric mantle, and lower crust (Richards, 2009; Grosjean et al., 2022). Coupled with extension and the reduced thickness of thin-intermediate arcs this would result in a focused, tectonic structure-controlled transfer of rather primitive and sometimes alkaline magmas to shallow levels for timescales sufficient to form giant and supergiant porphyry Cu–Au deposits.

6. Conclusions

Porphyry Cu–Au deposits are formed both in thick continental and in thin-intermediate oceanic to transitional crust arcs. Whereas all these deposits are characterized by similar mineralization processes at shallow depths, they display systematic differences of Au/Cu ratios and overall metal endowments that result from distinct precursor magma evolutions.

Porphyry Cu–Au deposits in thick arcs are characterized by low Au/Cu ratios and include the largest Cu-rich porphyry Cu–Au deposits (up to >100 Mt Cu). The model discussed above argues that Cu-rich porphyry Cu–Au deposits in thick arcs and their metal endowments and metal ratios can be explained through a two-stage process: (i) lower crustal (>20 km depth) accumulation of hybrid magmas, fluids and metals during several Myr and (ii) subsequent transfer of these H_2O-undersaturated magma to shallow levels where they exsolve aqueous fluids and metals.

In contrast, porphyry Cu–Au deposits in thin-intermediate arcs are characterized by high Au/Cu ratios and include the largest Au endowments (up to >2500 tons Au). These deposits as well as their metal endowments and metal ratios can be explained by little differentiated mantle-derived magmas that ascend to shallow crustal levels where they exsolve aqueous fluids and metals.

These end-member settings of fluid and metal exsolution are intrinsically linked to the different crustal thicknesses of continental versus oceanic arcs. Ultimately, this shows that any arc magma may form a porphyry Cu–Au deposit but the crustal architecture in which it occurs will determine the metal endowments and metal ratios of the deposit through the processes discussed above.

The model here proposed is a simplification of the multistage, cumulative processes leading to the formation of economic porphyry Cu–Au deposits. Additional processes could be at work, e.g., Cu- and Au-rich sulfide recycling (Shafiei et al., 2008; Richards, 2009; Xu et al., 2021; Holwell et al., 2022), and tapping of fertile mantle domains (Holwell et al., 2019): some mismatch between real data and simulations (e.g., Figs. 8a–c) supports this possibility. Nonetheless, the overall promising fit between model and real Cu and Au endowments and Cu/Au ratios suggests that the two distinct processes here proposed are viable first-order explanations of the formation of porphyry Cu–Au deposits in thin versus thick arcs. This recognition should assist the refinement of petrological and geochemical tools to explore these different geodynamic settings.

CRediT authorship contribution statement

Conceptualization, methodology, interpretation, writing and visualization were carried out by MC.

Declaration of competing interest

The authors declare that they have no known competing financial interests or personal relationships that could have appeared to influence the work reported in this paper.

Data availability

All data, code, and materials used in this work are available in the main text or the Supplementary Material.

Acknowledgements

I would like to thank Jeff Hedenquist and an anonymous reviewer for constructive and stimulating reviews as well as Rosemary Hickey-Vargas for efficient editorial handling.

Funding

This study was funded by the Swiss National Science Foundation (grant N. 200021_169032 to MC).

Author contributions

Conceptualization, methodology, interpretation, writing and visualization were carried out by MC.

Appendix A. Supplementary material

Supplementary material related to this article can be found online at https://doi.org/10.1016/j.epsl.2022.117864.

References

Annen, C., 2009. From plutons to magma chambers: thermal constraints on the accumulation of eruptible silicic magma in the upper crust. Earth Planet. Sci. Lett. 284, 409–416. https://doi.org/10.1016/j.epsl.2009.05.006.

Annen, C., Blundy, J.D., Sparks, R.S.J., 2006. The genesis of intermediate and silicic magmas in deep crustal hot zones. J. Petrol. 47, 505–539. https://doi.org/10.1093/petrology/egi084.

Arribas Jr, A., Hedenquist, J.W., Itaya, T., Okada, T., Concepción, R.A., Garcia Jr., J.S., 1995. Contemporaneous formation of adjacent porphyry and epithermal Cu–Au deposits over 300 ka in northern Luzon, Philippines. Geology 23, 337–340. https://doi.org/10.1130/0091-7613(1995)023<0337:CFOAPA>2.3.CO;2.

Ballard, J.R., Palin, J.M., Williams, I.S., Campbell, I.H., Faunes, A., 2001. Two ages of porphyry intrusion resolved for the super-giant Chuquicamata copper deposit of northern Chile by ELA-ICP-MS and SHRIMP. Geology 29, 383–386. https://doi.org/10.1130/0091-7613(2001)029<0383:TAOPIR>2.0.CO;2.

Bertrand, G., Guillou-Frottier, L., Loiselet, C., 2014. Distribution of porphyry copper deposits along the western Tethyan and Andean subduction zones: insights from a paleotectonic approach. Ore Geol. Rev. 60, 174–190.

Braxton, D.P., Cooke, D.R., Dunlap, J., Norman, M., Reiners, P., Stein, H., Waters, P., 2012. From crucible to graben in 2.3 Ma: a high-resolution geochronological study of porphyry life cycles, Boyongan-Bayugo copper-gold deposits, Philippines. Geology 40, 471–474. https://doi.org/10.1130/G33125.1.

Buret, Y., von Quadt, A., Heinrich, C., Selby, D., Wälle, M., Peytcheva, I., 2016. From a long-lived upper-crustal magma chamber to rapid porphyry copper emplacement: reading the geochemistry of zircon crystals at Bajo de la Alumbrera (NW Argentina). Earth Planet. Sci. Lett. 450, 120–131. https://doi.org/10.1016/j.epsl.2016.06.017.

Burrows, D.R., Rennison, M., Burt, D., Davies, R., 2020. The onto Cu–Au discovery, Eastern Sumbawa, Indonesia: a large, middle Pleistocene lithocap-hosted high-sulfidation covellite-pyrite porphyry deposit. Econ. Geol. 115, 1385–1412. https://doi.org/10.5382/econgeo.4766.

Cannell, J., Cooke, D.R., Walshe, J.L., Stein, H., 2005. Geology, mineralization, alteration, and structural evolution of the El Teniente Porphyry Cu–Mo deposit. Econ. Geol. 100, 979–1003. https://doi.org/10.2113/gsecongeo.100.5.979.

Cashman, K.V., Sparks, R.S.J., Blundy, J.D., 2017. Vertically extensive and unstable magmatic systems: a unified view of igneous processes. Science 355. https://doi.org/10.1126/science.aag3055.

Cembrano, J., Lara, L., 2009. The link between volcanism and tectonics in the southern volcanic zone of the Chilean Andes: a review. Tectonophysics 471, 96–113. https://doi.org/10.1016/j.tecto.2009.02.038.

Chelle-Michou, C., Chiaradia, M., Ovtcharova, M., Ulianov, A., Wotzlaw, J.-F., 2014. Zircon petrochronology reveals the temporal link between porphyry systems and the magmatic evolution of their hidden plutonic roots (the Eocene Coroccohuayco deposit, Peru). Lithos 198–199, 129–140. https://doi.org/10.1016/j.lithos.2014.03.017.

Chelle-Michou, C., Chiaradia, M., Selby, D., Ovtcharova, M., Spikings, R.A., 2015. High-resolution geochronology of the Coroccohuayco Porphyry-Skarn deposit, Peru: a rapid product of the Incaic Orogeny. Econ. Geol. 110, 423–443. https://doi.org/10.2113/econgeo.110.2.423.

Chelle-Michou, C., Rottier, B., Caricchi, L., Simpson, G., 2017. Tempo of magma degassing and the genesis of porphyry copper deposits. Sci. Rep. 7, 40566. https://doi.org/10.1038/srep40566.

Chiaradia, M., 2021a. Magmatic controls on metal endowments of porphyry Cu–Au deposits. SEG Spec. Publ. 24, 1–16.

Chiaradia, M., 2021b. Zinc systematics quantify crustal thickness control on fractionating assemblages of arc magmas. Sci. Rep. 11, 14667. https://doi.org/10.1038/s41598-021-94290-6.

Chiaradia, M., 2020. Gold endowments of porphyry deposits controlled by precipitation efficiency. Nat. Commun. 11, 248. https://doi.org/10.1038/s41467-019-14113-1.

Chiaradia, M., 2015. Crustal thickness control on Sr/Y signatures of recent arc magmas: an Earth scale perspective. Sci. Rep. 5, 8115. https://doi.org/10.1038/srep08115.

Chiaradia, M., 2014. Copper enrichment in arc magmas controlled by overriding plate thickness. Nat. Geosci. 7, 43–46. https://doi.org/10.1038/ngeo2028.

Chiaradia, M., Caricchi, L., 2022. Supergiant porphyry copper deposits are failed large eruptions. Commun. Earth Environ. 3, 1–9. https://doi.org/10.1038/s43247-022-00440-7.

Chiaradia, M., Caricchi, L., 2017. Stochastic modelling of deep magmatic controls on porphyry copper deposit endowment. Sci. Rep. 7, 44523. https://doi.org/10.1038/srep44523.

Chiaradia, M., Merino, D., Spikings, R., 2009. Rapid transition to long-lived deep crustal magmatic maturation and the formation of giant porphyry-related mineralization (Yanacocha, Peru). Earth Planet. Sci. Lett. 288, 505–515. https://doi.org/10.1016/j.epsl.2009.10.012.

Chiaradia, M., Ulianov, A., Kouzmanov, K., Beate, B., 2012. Why large porphyry Cu deposits like high Sr/Y magmas? Sci. Rep. 2, 685. https://doi.org/10.1038/srep00685.

Clark, A.H., 1993. Are outsize porphyry copper deposits either anatomically or environmentally distinctive? Soc. Econ. Geol. Spec. Publ. 2, 213–283.

Cloos, M., 2001. Bubbling magma chambers, cupolas, and porphyry copper deposits. Int. Geol. Rev. 43, 285–311.

Cooke, D.R., Hollings, P., Walshe, J.L., 2005. Giant porphyry deposits: characteristics, distribution, and tectonic controls. Econ. Geol. 100, 801–818. https://doi.org/10.2113/gsecongeo.100.5.801.

Deckart, K., Clark, A.H., Cuadra, P., Fanning, M., 2013. Refinement of the time-space evolution of the giant Mio-Pliocene Río Blanco-Los Bronces porphyry Cu–Mo cluster, Central Chile: new U–Pb (SHRIMP II) and Re–Os geochronology and 40Ar/39Ar thermochronology data. Miner. Depos. 48, 57–79. https://doi.org/10.1007/s00126-012-0412-9.

Dilles, J.H., Stein, H.J., Martin, M.W., 2004. Re–Os and U–Pb ages for the duration of the giant Butte, Montana, porphyry Cu–Mo and Cordilleran base metal lode ore deposit.

Fiorentini, M.L., Garwin, S.L., 2010. Evidence of a mantle contribution in the genesis of magmatic rocks from the Neogene Batu Hijau district in the Sunda Arc, South Western Sumbawa, Indonesia. Contrib. Mineral. Petrol. 159, 819–837. https://doi.org/10.1007/s00410-009-0457-7.

Fiorentini, M.L., LaFlamme, C., Denyszyn, S., Mole, D., Maas, R., Locmelis, M., Caruso, S., Bui, T.-H., 2018. Post-collisional alkaline magmatism as gateway for metal and sulfur enrichment of the continental lower crust. Geochim. Cosmochim. Acta 223, 175–197. https://doi.org/10.1016/j.gca.2017.11.009.

Fortin, M.-A., Riddle, J., Desjardins-Langlais, Y., Baker, D.R., 2015. The effect of water on the sulfur concentration at sulfide saturation (SCSS) in natural melts. Geochim. Cosmochim. Acta 160, 100–116. https://doi.org/10.1016/j.gca.2015.03.022.

Garwin, S., 2002. The geologic setting of intrusion-related hydrothermal systems near the Batu Hijau porphyry copper-gold deposit. Sumbawa, Indonesia. https://doi.org/10.5382/SP.09.15.

Grosjean, M., Moritz, R., Rezeau, H., Hovakimyan, S., Ulianov, A., Chiaradia, M., Melkonyan, R., 2022. Arabia-Eurasia convergence and collision control on Cenozoic juvenile K-rich magmatism in the South Armenian block, Lesser Caucasus. Earth-Sci. Rev. 226, 103949. https://doi.org/10.1016/j.earscirev.2022.103949.

Hall, R., 2002. Cenozoic geological and plate tectonic evolution of SE Asia and the SW Pacific: computer-based reconstructions, model and animations. J. Asian Earth Sci. 20, 353–431. https://doi.org/10.1016/S1367-9120(01)00069-4.

Hao, H., Park, J.-W., Campbell, I.H., 2022. Role of magma differentiation depth in controlling the Au grade of giant porphyry deposits. Earth Planet. Sci. Lett. 593, 117640. https://doi.org/10.1016/j.epsl.2022.117640.

Hildreth, W., Moorbath, S., 1988. Crustal contributions to arc magmatism in the Andes of central Chile. Contrib. Mineral. Petrol. 98, 455–489. https://doi.org/10.1007/BF00372365.

Holwell, D.A., Fiorentini, M., McDonald, I., Lu, Y., Giuliani, A., Smith, D.J., Keith, M., Locmelis, M., 2019. A metasomatized lithospheric mantle control on the metallogenic signature of post-subduction magmatism. Nat. Commun. 10, 3511. https://doi.org/10.1038/s41467-019-11065-4.

Holwell, D.A., Fiorentini, M.L., Knott, T.R., McDonald, I., Blanks, D.E., Campbell McCuaig, T., Gorczyk, W., 2022. Mobilisation of deep crustal sulfide melts as a first order control on upper lithospheric metallogeny. Nat. Commun. 13, 573. https://doi.org/10.1038/s41467-022-28275-y.

Jensen, E.P., Barton, M.D., 2000. Gold deposits related to alkaline magmatism. https://doi.org/10.5382/Rev.13.08.

Kay, S.M., Mpodozis, C., Tittler, A., Cornejo, P., 1994. Tertiary magmatic evolution of the maricunga mineral belt in Chile. Int. Geol. Rev. 36, 1079–1112. https://doi.org/10.1080/00206819409465506.

Large, S.J.E., Quadt, A., von Wotzlaw, J.-F., Guillong, M., Heinrich, C.A., 2018. Magma evolution leading to porphyry Au–Cu mineralization at the Ok Tedi deposit, Papua New Guinea: trace element geochemistry and high-precision geochronology of igneous zircon. Econ. Geol. 113, 39–61.

Leys, C.A., Cloos, M., New, B.T.E., MacDonald, G.D., 2012. Copper-gold ± molybdenum deposits of the ertsberg-grasberg district. Papua, Indonesia. https://doi.org/10.5382/SP.16.10.

Li, Y., Audétat, A., 2013. Gold solubility and partitioning between sulfide liquid, monosulfide solid solution and hydrous mantle melts: implications for the formation of Au-rich magmas and crust–mantle differentiation. Geochim. Cosmochim. Acta 118, 247–262. https://doi.org/10.1016/j.gca.2013.05.014.

Li, Y., Audétat, A., Liu, Z., Wang, F., 2021. Chalcophile element partitioning between Cu-rich sulfide phases and silicate melt and implications for the formation of Earth's continental crust. Geochim. Cosmochim. Acta 302, 61–82. https://doi.org/10.1016/j.gca.2021.03.020.

Li, Y., Feng, L., Kiseeva, E.S., Gao, Z., Guo, H., Du, Z., Wang, F., Shi, L., 2019. An essential role for sulfur in sulfide-silicate melt partitioning of gold and magmatic gold transport at subduction settings. Earth Planet. Sci. Lett. 528, 115850. https://doi.org/10.1016/j.epsl.2019.115850.

Loucks, R., 2012. Chemical characteristics, geodynamic settings, and petrogenesis of gold-ore-forming arc magmas. CET Q. N. 20, 4–12.

Loucks, R.R., 2014. Distinctive composition of copper-ore-forming arc magmas. Aust. J. Earth Sci. 61, 5–16. https://doi.org/10.1080/08120099.2013.865676.

Mantle, G.W., Collins, W.J., 2008. Quantifying crustal thickness variations in evolving orogens: correlation between arc basalt composition and Moho depth. Geology 36, 87–90. https://doi.org/10.1130/G24095A.1.

Marsh, T.M., Einaudi, M.T., McWilliams, M., 1997. 40 Ar/39 Ar geochronology of Cu–Au and Au–Ag mineralization in the Potrerillos District, Chile. Econ. Geol. 92, 784–806. https://doi.org/10.2113/gsecongeo.92.7-8.784.

Matjuschkin, V., Blundy, J.D., Brooker, R.A., 2016. The effect of pressure on sulphur speciation in mid- to deep-crustal arc magmas and implications for the formation of porphyry copper deposits. Contrib. Mineral. Petrol. 171, 66. https://doi.org/10.1007/s00410-016-1274-4.

Mercer, C.N., Reed, M.H., Mercer, C.M., 2015. Time scales of porphyry Cu deposit formation: insights from titanium diffusion in quartz. Econ. Geol. 110, 587–602. https://doi.org/10.2113/econgeo.110.3.587.

Moss, R., Scott, S.D., Binns, R.A., 2001. Gold content of eastern manus basin volcanic rocks: implications for enrichment in associated hydrothermal precipitates. Econ. Geol. 96, 91–107. https://doi.org/10.2113/gsecongeo.96.1.91.

Mungall, J.E., Brenan, J.M., Godel, B., Barnes, S.J., Gaillard, F., 2015. Transport of metals and sulphur in magmas by flotation of sulphide melt on vapour bubbles. Nat. Geosci. 8, 216–219. https://doi.org/10.1038/ngeo2373.

Newman, S., Lowenstern, J.B., 2002. VolatileCalc: a silicate melt–H2O–CO2 solution model written in Visual Basic for excel. Comput. Geosci. 28, 597–604.

Park, J.-W., Campbell, I.H., Chiaradia, M., Hao, H., Lee, C.-T., 2021. Crustal magmatic controls on the formation of porphyry copper deposits. Nat. Rev. Earth Environ. 2, 542–557. https://doi.org/10.1038/s43017-021-00182-8.

Park, J.-W., Campbell, I.H., Malaviarachchi, S.P.K., Cocker, H., Hao, H., Kay, S.M., 2019. Chalcophile element fertility and the formation of porphyry Cu ± Au deposits. Miner. Depos. 54, 657–670. https://doi.org/10.1007/s00126-018-0834-0.

Parra-Avila, L.A., Hammerli, J., Kemp, A.I.S., Rohrlach, B., Loucks, R., Lu, Y., Williams, I.S., Martin, L., Roberts, M.P., Fiorentini, M.L., 2022. The long-lived fertility signature of Cu–Au porphyry systems: insights from apatite and zircon at Tampakan, Philippines. Contrib. Mineral. Petrol. 177, 18. https://doi.org/10.1007/s00410-021-01878-2.

Plank, T., Kelley, K.A., Zimmer, M.M., Hauri, E.H., Wallace, P.J., 2013. Why do mafic arc magmas contain ∼4wt% water on average? Earth Planet. Sci. Lett. 364, 168–179. https://doi.org/10.1016/j.epsl.2012.11.044.

Pollard, P.J., Jongens, R., Stein, H., Mark Fanning, C., Smillie, R., 2021. Rapid formation of porphyry and skarn copper-gold mineralization in a postsubduction environment: Re–Os and U–Pb geochronology of the Ok Tedi Mine, Papua New Guinea. Econ. Geol. 116, 533–558. https://doi.org/10.5382/econgeo.4799.

Profeta, L., Ducea, M.N., Chapman, J.B., Paterson, S.R., Gonzales, S.M.H., Kirsch, M., Petrescu, L., DeCelles, P.G., R Core Team, 2015. Quantifying crustal thickness over time in magmatic arcs. Scientific Reports, vol. 5, p. 17786.

R Core Team. R: A language and environment for statistical computing. R Foundation for Statistical Computing, Vienna, Austria.

Rabbia, O.M., Correa, K.J., Hernández, L.B., Ulrich, T., 2017. "Normal" to adakite-like arc magmatism associated with the El Abra porphyry copper deposit, Central Andes, Northern Chile. Int. J. Earth Sci. (Geol. Rundsch.) 106, 2687–2711. https://doi.org/10.1007/s00531-017-1454-0.

Redmond, P.B., Einaudi, M.T., 2010. The Bingham Canyon porphyry Cu–Mo–Au deposit. I. Sequence of intrusions, vein formation, and sulfide deposition. Econ. Geol. 105, 43–68. https://doi.org/10.2113/gsecongeo.105.1.43.

Reich, M., Parada, M.A., Palacios, C., Dietrich, A., Schultz, F., Lehmann, B., 2003. Adakite-like signature of Late Miocene intrusions at the Los Pelambres giant porphyry copper deposit in the Andes of central Chile: metallogenic implications. Miner. Depos. 38, 876–885. https://doi.org/10.1007/s00126-003-0369-9.

Richards, J.P., 2021. Porphyry copper deposit formation in arcs: what are the odds? Geosphere 18, 130–155. https://doi.org/10.1130/GES02086.1.

Richards, J.P., 2013. Giant ore deposits formed by optimal alignments and combinations of geological processes. Nat. Geosci. 6, 911–916. https://doi.org/10.1038/ngeo1920.

Richards, J.P., 2011. High Sr/Y arc magmas and porphyry Cu ± Mo ± Au deposits: just add water. Econ. Geol. 106, 1075–1081. https://doi.org/10.2113/econgeo.106.7.1075.

Richards, J.P., 2009. Postsubduction porphyry Cu–Au and epithermal Au deposits: products of remelting of subduction-modified lithosphere. Geology 37, 247–250. https://doi.org/10.1130/G25451A.1.

Richards, J.P., 2003. Tectono-magmatic precursors for porphyry Cu–(Mo–Au) deposit formation. Econ. Geol. 98, 1515–1533. https://doi.org/10.2113/gsecongeo.98.8.1515.

Ripley, E.M., Brophy, J.G., Li, C., 2002. Copper solubility in a basaltic melt and sulfide liquid/silicate melt partition coefficients of Cu and Fe. Geochim. Cosmochim. Acta 66, 2791–2800. https://doi.org/10.1016/S0016-7037(02)00872-4.

Rock, N.M.S., Groves, D.I., 1988. Do lamprophyres carry gold as well as diamonds? Nature 332, 253–255. https://doi.org/10.1038/332253a0.

Schöpa, A., Annen, C., 2013. The effects of magma flux variations on the formation and lifetime of large silicic magma chambers. J. Geophys. Res., Solid Earth 118, 926–942. https://doi.org/10.1002/jgrb.50127.

Shafiei, B., Haschke, M., Shahabpour, J., 2008. Recycling of orogenic arc crust triggers porphyry Cu mineralization in Kerman Cenozoic arc rocks, southeastern Iran. Miner. Depos. 44, 265. https://doi.org/10.1007/s00126-008-0216-0.

Sillitoe, R.H., 2010. Porphyry copper systems*. Econ. Geol. 105, 3–41. https://doi.org/10.2113/gsecongeo.105.1.3.

Sillitoe, R.H., 2000. Gold-rich porphyry deposits: descriptive and genetic models and their role in exploration and discovery. https://doi.org/10.5382/Rev.13.09.

Sillitoe, R.H., 1973. The tops and bottoms of porphyry copper deposits. Econ. Geol. 68, 799–815.

Stein, H.J., Markey, R., Sillitoe, R.H., Perelló, J., 2002. Defining the lifespan of a giant porphyry Cu deposit: Re–Os dating at Los Pelambres, Chile. Geochim. Cosmochim. Acta 66 (Supplement 1), 738.

Stern, C.R., Skewes, M.A., Arévalo, A., 2011. Magmatic evolution of the giant El Teniente Cu–Mo deposit, Central Chile. J. Petrol. 52, 1591–1617. https://doi.org/10.1093/petrology/egq029.

Tapster, S., Condon, D.J., Naden, J., Noble, S.R., Petterson, M.G., Roberts, N.M.W., Saunders, A.D., Smith, D.J., 2016. Rapid thermal rejuvenation of high-crystallinity magma linked to porphyry copper deposit formation; evidence from the Koloula Porphyry Prospect, Solomon Islands. Earth Planet. Sci. Lett. 442, 206–217. https://doi.org/10.1016/j.epsl.2016.02.046.

Vaca, S., Garwin, S., Whistler, B., Ward, J., Mather, N., Cruz, A., Guerrero, N., Guachamín, A., 2019. Lithochemistry of the Alpala Cu–Au Porphyry Deposit, northern Andes of Ecuador.

Wallace, P.J., 2005. Volatiles in subduction zone magmas: concentrations and fluxes based on melt inclusion and volcanic gas data. J. Volcanol. Geotherm. Res. 140, 217–240. https://doi.org/10.1016/j.jvolgeores.2004.07.023.

Wilkinson, J.J., 2013. Triggers for the formation of porphyry ore deposits in magmatic arcs. Nat. Geosci. 6, 917–925. https://doi.org/10.1038/ngeo1940.

Xu, B., Hou, Z.-Q., Griffin, W.L., Lu, Y., Belousova, E., Xu, J.-F., O'Reilly, S.Y., 2021. Recycled volatiles determine fertility of porphyry deposits in collisional settings. Am. Mineral. 106, 656–661. https://doi.org/10.2138/am-2021-7714.

Zimmerman, A., Stein, H.J., Morgan, J.W., Markey, R.J., Watanabe, Y., 2014. Re–Os geochronology of the El Salvador porphyry Cu–Mo deposit, Chile: tracking analytical improvements in accuracy and precision over the past decade. Geochim. Cosmochim. Acta 131, 13–32. https://doi.org/10.1016/j.gca.2014.01.016.